Dynamic regulation of neuronal Vault trafficking and RNA cargo by the noncoding RNA, Vaultrc5

Mason R. B. Musgrove[1*], Laura J. Leighton[2], Wei-Siang Liau[1], Alexander D. Walsh[1], Paul R. Marshall[1,3], Stephanie M. Heyworth[1,4] Adekunle T. D. Bademosi[1], Nathalie Hertrich[5], Qiongyi Zhao[1], Sachithrani U. Madugalle[1], Ambika Periyakaruppiah[1], Xiang Li[6], Joshua W. A. Davies[1,3], Haobin Ren[1], Hao Gong[1], Frederic Meunier[1], Marina Mikhaylova[5], and Timothy W. Bredy[1#]

[1]Centre for RNA in Neuroscience, Queensland Brain Institute, University of Queensland, Brisbane, QLD Australia; [2]Australian Institute for Bioengineering and Nanotechnology, University of Queensland: [3]John Curtin School for Medical Research, Australian National University, Canberra, ACT Australia: [4]School of the Environment, University of Queensland, Brisbane, QLD Australia; [5]Institute for Biology, Humboldt University, Berlin, Germany; [6]Zhongnan Hospital, Wuhan University, Wuhan, China.

Please send correspondence to

Prof Timothy Bredy: t.bredy@uq.edu.au

Keywords: Vaults, Vaultrc5, RNA localisation, Fear learning

Abstract

Vaults are large ribonucleoprotein complexes of unknown function in neurons. Here, we report that the Vault-associated noncoding RNA, Vaultrc5, is highly enriched at the synapse and is required for activity-dependent Vault trafficking in neurons. We have discovered that Vaults are comprised of unique populations of coding and non-coding RNA, and that this cargo varies dynamically between subcellular compartments. In addition, Vaultrc5 knockdown at the synapse shifts the RNA cargo toward transcripts associated with immune surveillance, and Vaultrc5 knockdown, *in vivo,* leads to impaired fear learning. These findings suggest that the Vaultrc5 is critically involved in coordinating the experience-dependent trafficking of Vaults and related RNA cargo, which represents a novel feature of neuronal plasticity underlying learning and memory.

Introduction

It is well established that neuronal RNAs are differentially expressed and localised in response to activity, particularly those that are active at the synapse (Hirokawa, 2006; Sossin & DesGroseillers, 2006). RNA localisation is required for synaptic plasticity, as it allows for the translation of synaptic RNA pools in response to learning induced synaptic activity that support memory formation (Doyle & Kiebler, 2011; Hirokawa, 2006; Kang & Schuman, 1996). However, the selective packaging, synaptic targeting, and translation of synapse-destined RNA is poorly understood (Rangaraju et al., 2017).

RNA is typically transported in ribonucleoprotein (RNP) particles called trafficking granules (Kiebler & DesGroseillers, 2000; Steiner et al., 2006). Due to the size of these granules, their formation most likely occurs in the cytoplasm via polyribosomes. Since trafficking granules bind motor proteins on microtubules to move their cargo throughout the cell, how and where trafficking granules form is vital for regulating synaptic plasticity (Antar et al., 2005; Chen et al., 2006; Knowles et al., 1996). After trafficking, mRNAs are translated at polyribosomes in presynaptic actin-rich endoplasmic reticulum-like patches, and ncRNA are either immediately functionalised or packaged into extracellular vesicles for transmission (Koenig et al., 2000; Mathur et al., 2018; Steward & Levy, 1982). Thus, RNA trafficking and local translation is required for synaptic plasticity, which is, in turn required for long-term memory. Revealing the complete repertoire of synapse-enriched RNAs, how they are trafficked, and when this occurs is therefore paramount to understanding brain function.

Vaults are large 13 MDa ribonucleoproteins that are highly conserved across Eukarya, resemble cages, and transit between the neuron soma and synapse. However, the functional relevance of Vaults in neurons is largely unexplored. Major vault protein (MVP) is the main constituent and is vital for vault structure, with protein structure studies implicating pH as an opening signal thanks to MVP's EF-hand motif (Paspalas et al., 2009; Poderycki et al., 2006; van Zon et al., 2002) and the non-coding RNA Vaultrc5 is the only known RNA component. Due to the Vault's characteristics, and multiple studies indicating that MVP and Vaultrc5 may be associated with synaptic plasticity, we hypothesised that vaults are a unique class of RNA trafficking granules (Wakatsuki et al., 2021).

Here, using a targeted RNA degradation platform to knock down Vaultrc5 combined with super resolution microscopy and sequencing, we have analysed the functional role of Vaultrc5 in the regulation of Vault trafficking and contents in primary cortical neurons, *in vitro*. We find that Vaults and Vaultrc5 RNA colocalise at the synapse, and that Vaultrc5 is required for Vault trafficking and mobility. Vault immunoprecipitation in activated primary cortical neurons followed by RNA sequencing revealed the unique cargo being trafficked between the nucleus and synapse. Vaultrc5 knockdown dramatically altered the RNA contents of Vaults in the synaptic compartment. Finally, in the adult brain, Vaultrc5 is also highly expressed in the synaptic compartment and is involved in plasticity and memory. These data indicate that neuronal Vaults are RNA trafficking granules that are heavily dependent on the activity of the noncoding RNA Vaultrc5, which suggest a novel mechanism of RNA localisation underlying plasticity and memory.

Methods

Reagent	Source	Catalogue number
Experimental models		
C57BL/6J E16 primary cortical neurons (*M. musculus*)	Jackson Laboratory	664
C57BL/6J 10-week old mice (*M. musculus*)	Jackson Laboratory	664
Recombinant DNA		
Mvp (NM_080638) Mouse Tagged ORF Clone	Origene	MG210985
pAMCBA-pL-WPRE-bGHpA-Cirtsvaultrc5	This study	N/A
pFSy1.1 GW-GFPT2ACirtsPinCalm3gRNABsmBI	This study	N/A
pFSy1.1 GW-MVPEOS	This study	N/A
pFSy1.1 MVPGFP	This study	N/A
pMD2.G	Didier Trono via Addgene	12259
pMDLg/pRRE	Didier Trono via Addgene	12251
pRSV-Rev	Didier Trono via Addgene	12253
Antibodies and molecular dyes		
Mouse monoclonal Anti-DDK (FLAG) tag	Origene	OTI4C5
Chicken polyclonal anti-Bassoon	Synaptic Systems	141016
Chicken polyclonal anti-β-tubulin-III	Synaptic Systems	302304
DAPI	Thermo Scientific	D1306
Goat polyclonal anti-MAP2	Santa Cruz	SC5359
Guinea pig polyclonal anti-Shank3	SYSY	162304
Mouse monoclonal (AP20) anti-MAP2 conjugated to Alexa 488	Merck-Millipore	MAB3418X
Mouse monoclonal anti-Bassoon	Enzo	ADI-VAM-PS003-F
Mouse monoclonal anti-Synaptophysin	Abcam	Ab8049
Mouse monoclonal anti-β-tubulin-III	Thermo Fisher Scientific	MA5-11732
Normal mouse IgG	Santa Cruz Biotech	Sc-2025
Rabbit polyclonal anti-GFP	Abcam	Ab6556
Rabbit polyclonal anti-MVP	ProteinTech	16478-1-AP
TO3-3PEG-Biotin Fluorophore	Abmgood	G7959
YO3-3PEG-Biotin Fluorophore	Abmgood	G7957
Oligonucleotides		

qPCR/dPCR primers	This study	Appendix
Chemicals, enzymes, and other reagents		
Custom buffers	This study	Appendix
175cm^2 flasks with filter cap	Corning	CLS431080
200mm polystyrene petri dish	Thermo Scientific	93150TS
6 & 12-well cell culture plate	Corning	CLS3516, CLS3513
Agencourt AMPure XP	Beckman Coulter	A63881
Agencourt RNAClean XP	Beckman Coulter	A63987
Benzonase	Sigma-Aldrich	E1014-25KU
Cell strainer 45µm	Falcon	352340
DMEM high glucose	Thermo Fisher	11995073
DMEM low glucose	Thermo Fisher	11965118
Double cannulae	Plastics One	Custom
DPBS, no calcium, no magnesium	Gibco	14190250
EvaGreen PCR Kit	Qiagen	250111
Fetal Bovine Serum	Gibco	FBSFR-S00FU
GlutaMax	Gibco	35050061
Lipofectamine 3000	Life Tech Australia	L3000150
Lysogeny broth	In-house	N/A
Mattek dish 35mm 20mm glass inset	Mattek	P35G-1.5-20-C
Nalgene polycarbonate centrifuge bottle	Thermo Scientific	3140-0250
Nalgene Rapid-Flow Sterile PES Filter (0.45µm, 50mm)	Thermo Scientific	09-740-63B
Neurobasal	Thermo Fisher	21103-049
NucleoZOL	Scientifix	740404.2
Opti-MEM	Thermo Fisher	31985-070
Papain	Sigma-Aldrich	P4762
Paraformaldehyde	Sigma-Aldrich	158127
PBS	In-house	N/A
Penicillin-streptomycin	Gibco	15140122
Polyallomer centrifuge tube (14x89mm)	Beckman Coulter	331372
Poly-L-Ornithine	Sigma-Aldrich	P2533-500MG
Potassium chloride 2M	Invitrogen	AM9640G
RNA Clean & Concentrate 200	Zymo Research	R1014
Sensi-FAST SYBR No-ROX Kit	Bioline	BIO-98020
Sodium chloride 0.9%	Pfizer	BN-3521340
Sucrose	Sigma-Aldrich	S9378
Software		
CutAdapt v3.7	https://cutadapt.readthedocs.io/en/v3.7/	
EdgeR v4.4.1	https://bioconductor.org/packages/release/bioc/html/edgeR.html	
FIJI – BIOP JaCoP	https://github.com/BIOP/ijp-jacop-b	
FIJI – KymographClear 2.0A	https://doi.org/10.1091/mbc.e15-06-0404	
FreezeFrame 4	Actimetrics	
HISAT2 v2.2.1	https://daehwankimlab.github.io/hisat2/	

HTSeq-count v2.0.5	https://htseq.readthedocs.io/en/latest/overview.html
Huygens Professional Deconvolution	Scientific Volume Imaging
Instruments	
10ul 1700 Series Gastight Syringe (Luer tip)	Harvard Apparatus
Abbelight SAFe 360	Single-molecule localisation microscope (SAFe 360; Abbelight), ECLIPSE Ti2 body (Nikon), 2x ORCA-Fusion BT sCMOS cameras (Hamamatsu),CFI APO TIRF 100XC/1.49 NA oil-immersion objective, NEO Imaging software (Abbelight).
Avanti J-26 XPI ultracentrifuge, JLA 16.250 rotor	Beckman Coulter
Fusion 100 Infusion Pump	Chemyx
L-100 XP ultracentrifuge, SW41Ti rotor	Beckman Coulter
Nanodrop Spectrophotometer	Thermo Scientific
NovaSeq 6000	Owned by GeneWiz, via Azenta
Olympus SpinSR10 Spinning Disk Confocal	CSU-W1 T2SSR confocal disk unit (Yokogawa Corp), IX83 body (Olympus), 2x ORCA-Fusion BT cameras (Hamamatsu), UPLXAPO60XO (NA 1.42, WD 0.15mm) objective, CellSens software (Olympus).
QIAcuity One 5-Plex	Qiagen
Qiagen Rotor-Gene Q	Qiagen
QuBit 4 Fluorescent Spectrophotometer	Invitrogen
STEDYCON microscope	Abbelight

Animals

Wild-type 10-week old C57BL/6J male mice (Australian Research Council (ARC)) were pair-housed in cages with a Plexiglas divider, and maintained on a 12-hour light/dark schedule and given *ad libitum* access to food and water. Testing was conducted during light phase in red light-illuminated testing rooms. All animal use and training, including embryos used for dissection, was in line with the Animal Ethics Committee of the University of Queensland and the Australian Code of Practice for the Care and Use of Animals for Scientific Purposes (eighth edition, 2013).

Construct generation

All constructs used the pFSyn(1.1)GW lentiviral expression vector (Addgene, #27232), which incorporates the rat synapsin 1 promoter, as a backbone. Each construct was verified with Sanger sequencing using custom primers (Appendix).

CRISPR-Inspired RNA Targeting System

The CIRTS cassette was sourced from the Dickinson laboratory at the University of Chicago, U.S.A. This cassette was PCR amplified and inserted between the AgeI and XbaI sites, with an NheI site generated upstream of XbaI (all New England Biolabs). Guide RNAs targeting Vaultrc5 or a scramble control of the respective guide were synthesised at Integrated DNA Technologies, then inserted into the XbaI site. CIRTS constructs were assayed for

knockdown efficacy and consistency in primary neurons using a combination of quantitative real-time PCR, and digital PCR.

RT-qPCR & dPCR

One microgram of RNA was synthesised into cDNA using the QuantiTect Reverse Transcription Kit (Qiagen) per the manufacturer's protocol. qPCR was performed on a RotoGeneQ (Qiagen) real-time PCR cycler with SensiFAST SYBR master mix (Bioline) and appropriate primers. Phosphoglycerate kinase I was used as an internal control. The threshold cycle for each experiment was chosen from the samples' linear range, and all samples normalised to the internal control using the ΔΔCT method. Each reaction was run in duplicate. Samples were then transferred to the QIAcuity One Digital PCR cycler for absolute quantification in 24-well, 26,000-partition plates (both Qiagen). PCR cycling parameters were identical to qPCR, and analysed as described below.

Mango4 aptamers

The Mango4 construct sequence was sourced from a paper by Autor et al. (2018)(Autour et al., 2018), and supplemented with the F30 scaffold from the same paper to minimise potential for steric hindrance. This Mango4::F30 insert was placed into the sequence of the respective RNA target at different locations, synthesised at IDT, then inserted between the BamHI (New England Biolabs) and XbaI sites. The inserts ordered from IDT included cleavable "tags" upstream and downstream of the BamHI and XbaI sites, respectively, to confirm restriction digestion. Ideal aptamers were determined by which produced the most consistent fluorescence and colocalization with known interacting partners during imaging.

Vault tagging

Major Vault Protein (MVP) was acquired already-fused at the C-terminus to Green Fluorescent Protein (eGFP) from Origene (MG210985), then cloned as the Mango4 aptamers without the cleavable tags mentioned.

Lentiviral production

All constructs were incorporated into individual lentiviral vectors using a third-generation packaging system: pMD2.3 (Addgene #12259), pRSV-REV (Addgene #12253), and pMDLg/pRRE (Addgene #12251). Plasmids were transfected per manufacturer's protocols using Lipofectamine 3000 (Thermo Fisher Scientific) into HEK293T cells at 80% confluency in culture medium: DMEM (Thermo Fisher Scientific #11965092), 1% GlutaMAX (#35050061), and 1% Penicillin-Streptomycin (#15140122) (both Gibco). After four hours, culture medium was supplemented with 10mM sodium pyruvate (Sigma-Aldrich #P2256), and 10mM sodium butyrate (Sigma-Aldrich #B5887) was added to inhibit cell growth. After fourty-eight hours incubation at 37°C and 5% CO2, virus was collected in 20% sucrose (Sigma-Aldrich #S0389) via ultracentrifugation. Titre was determined using the Lenti-X qRT-PCR Titration Kit (Takara Bio).

Lentiviral delivery & behavioural training

<u>Cannulation surgery</u>

Double cannulae (Plastics One) were implanted into the infralimbic prefrontal cortex in the anteroposterior plane along the midline. Implantation locations were centred at +1.8mm in

the anteroposterior, and -2.8mm in the dorsoventral plane. Mice were then placed into single housing conditions and given one week to recover prior to behavioural training.

Lentiviral infusion

Mice were fear conditioned, then given two 1µl lentivirus injections (1E7 – 1E8 IU/mL) through the cannulae over a forty-eight hour period. Sterile gas-tight 1700 series syringes (Harvard Apparatus) were used with the Fusion 100 Infusion pump (Chemyx) for this purpose.

Behavioural training

One week after infusion, mice were either extinction trained or exposed to context B for an equivalent time. Training and data analysis was performed as previously described, using 60 nonreinforced 120s CS presentations (Marshall et al., 2024).

Prefrontal cortex extraction

After behavioural training, animals were euthanised via cervical dislocation, and brains immediately extracted and placed on ice. Brains were then sliced into 40µm slices, or dounce-homogenized in a 2ml tissue grinder (Kimble Chase) and processed as appropriate per experiment.

Primary cortical neuron culture

E16 pregnant dams were euthanised via cervical dislocation, embryos extracted and euthanised via immersion in 4°C dissecting medium. Cortical tissue was extracted from embryonic day 16 embryos by removing the skull and meninges with fine-tipped tweezers. Neurons were added to neuronal culture medium: Neurobasal (Thermo Fisher Scientific, #21103049) containing 10% fetal bovine serum (Gibco #26140079) and 1% penicillin-streptomycin, which was supplemented with papain (#P4762) and benzonase (#E1014) (both Sigma-Aldrich). This mixture was incubated at 37°C for twenty minutes before homogenisation via gentle pipetting, then passed through a 40µm cell strainer (BD Falcon). Neurons were plated on well-plates or dishes coated for twenty-four hours with 1.2mM poly-L-ornithine (#P4957), 100mM boric acid (#B0349), 25mM sodium tetrahydroborate (#213462), 75mM sodium chloride (#S9888) (all Sigma-Aldrich) in ultrapure water. Culture medium was added and supplemented with B-27 (Invitrogen #17504), then replaced twenty-four hours later, and neurons were cultured at 37°C and 5% CO2 for seven to fourteen days prior to fixation or RNA extraction. Lentivirus was applied at DIV2 where appropriate.

Synaptosome preparation

Primary cortical neurons at DIV7 from 100mm tissue culture dishes (Falcon) were fixed with 1% methanol-free paraformaldehyde (Thermo Scientific #289206), then dissociated via incubation with StemPro Accutase (Invitrogen #00455556). Neurons were then pelleted in washing buffer, and synaptosomes prepared as previously described(Dunkley et al., 2008)**.** Unlike previous experiments, the sample was split into “cytoplasmic” and “perisynaptic” fractions by pooling and retaining the nuclear and cellular debris fractions generated across the experiment.

Vault immunoprecipitation

Primary cortical neurons transduced with the MVP::GFP, and Vaultrc5 CIRTS lentivirus constructs, were extracted as described above, and either processed as neurons or turned into synaptosomes. Dynabeads Protein G (Invitrogen #10003D) were resuspended in native lysis buffer: 25mM tris-hydrochloride (Roche #10812846001), 150mM potassium chloride (Sigma-Aldrich #P3911), 1% triton X-100 (Sigma-Aldrich #X100), 5mM EDTA (Bioworld #40520000), 5mM DTT (Thermo Scientific #R0861), 2.5ul/ml RNaseOut (Invitrogen #10777019), 1X Halt Protease Inhibitor Cocktail (Thermo Scientific, #78438). Beads were added to the samples and left to rotate for thirty minutes at 4°C. Next, fresh protein G beads were incubated for ten minutes with 5µg of either mouse anti-GFP (abcam #ab6556) or mouse immunoglobin G (Diagenode #C15200001) in native lysis buffer. These bead-bound antibodies were added to the samples and left to rotate for one hour at 4°C. On a magnet, each sample was washed several times with native lysis buffer, then low, and high salt buffers: 0.2X SSPE (Sigma-Aldrich #S2015), 1mM EDTA, 0.05% TWEEN-20 (Sigma-Aldrich #P1379) for low salt, plus 137.5mM sodium chloride for high salt, and 5mM DTT, 2.5ul/ml RNaseOut, 1X Halt Protease Inhibitor Cocktail. After final washes in native lysis buffer, samples were resuspended in 33ul reverse crosslinking buffer: 6% w/v lauroyl sarcosine (Sigma-Aldrich #L5125), 5mM EDTA, 5mM DTT, 1ul/sample RNaseOut, 0.8U/ml proteinase K (New England Biolabs, #P8107), in DPBS (Gibco #14190144). Samples were then incubated for one hour at 42°C, and one hour at 55°C.

RNA extraction

Each sample was incubated with Agencourt RNAClean XP Beads (Beckman Coulter) for ten minutes, allowed to clear on a magnet, then washed twice with 80% ethanol. Samples were dried at 37°C for four minutes, then incubated in ultrapure water for a further ten minutes to retrieve the sample as supernatant. DNase I (Zymo Research, #E1010) was then applied for ten minutes, and samples incubated for ten minutes with fresh RNAClean beads. After clearing on a magnet for ten minutes, a further two washes were performed with 80% ethanol. Beads were then dried and resuspended in ultrapure water as before, and supernatant retrieved. Resulting RNA was quantified using the QuBit 4 Fluorometer (Invitrogen) while the Qubit RNA High Sensitivity Kit, and RNA Integrity Score (RIN) was assessed using the Agilent 2100 Bioanalyser with the Agilent RNA 6000 Pico Kit.

Sequencing

Short-read sequencing was performed in a single lane on an Illumina MiSeq or NovaSeq using the Takara SMARTer Stranded Pico Input Mammalian v2 kit, per the manufacturer's instructions. Briefly, RNA samples were reverse-transcribed using first-strand cDNA synthesis, ribodepleted, purified using AMPure XP beads (Beckman Coulter), individually barcoded, and amplified for 16 cycles before final purification. Library profiles were analysed on the Agilent Bioanalyser 6000 using the DNA 1000 kit (both Agilent), and then pooled to a single sample at a concentration of 20Nm. An additional purification step was used to remove excess adapter dimer prior to running the sample.

Imaging

<u>Immunohistochemistry</u>

Primary cortical neurons plated on coated 35mm glass discs were fixed in 4% w/v paraformaldehyde (Sigma-Aldrich, #158127) for 10 minutes at room temperature, then permeabilised in PBS containing 0.2% Triton X-100 (Sigma-Aldrich, #93443). Samples were

washed several times, then blocked using in this buffer plus 10% donkey serum (Sigma-Aldrich, D9663) for one hour at room temperature. Primary antibodies were added at 1:1000, and incubated overnight at 4°C. Samples were washed as before, then incubated with secondary antibodies for one hour at room temperature, and either sealed on microscopy slides using nail polish or stored in PBS at 4°C.

Live microscopy

Primary cortical neurons plated on coated 35mm dishes were transduced at DIV2 with lentiviruses as appropriate. At DIV7, culture medium was exchanged for buffer containing 15mM HEPES, 145mM sodium chloride, 2.2mM calcium chloride, 0.5mM magnesium chloride, 5.6mM D-glucose (#G8270), 0.5mM ascorbic acid (all Sigma-Aldrich), and 0.1% bovine serum albumin (Invitrogen, #AM2616) in ultrapure water. Neurons were imaged at 37°C and 5% CO2, with and without stimulating with 56mM potassium chloride. Where appropriate, neurons were pre-incubated for ten minutes with YO3-3PEG-Biotin fluorophore (abmgood, #G957).

Stimulated emission depletion (STED) microscopy

Neurons plated and fixed on 35mm glass discs as described were imaged dry on a STEDYCON microscope (Aberrior) using an 100X oil objective (1.45 NA). STED utilised pulsed 775nm and 405nm lasers for depletion and excitation, respectively. Detector time gates were set between 0.5-6ns depending on wavelength.

Spinning-disc confocal microscopy

Neurons plated as above were kept in buffer per the live microscopy section at room temperature. These were imaged on an Olympus SpinSR10 Spinning Disk confocal controlled by Zeiss imaging software. Images were taken using the CSU-W1 T2SSR confocal disk unit at 1x zoom with an 100x oil immersion objective (UPLXAPO100X0, 1.45 NA). Z-stacks were generated with a step of 0.5µm, resulting in 15-20 slices each.

Superresolution microscopy

Neurons plated as above and kept as per the live microscopy section were imaged on an Abbelight SAFe 360 inverted single-molecule localisation microscope controlled by Abbelight NEO software. Video was taken using an ORCA-Fusion BT sCMOS cameras with an 100x oil immersion objective (Nikon CFI Apo TIRF, 1.49 NA). Parameters were 16,000 frames in a 256 x 256 format, at approx. 50fps using a 120mW 488nm laser at 30% power.

Experimental design and statistical analysis

The fear learning experiment was carried out with twelve animals per group, as power calculations within our previous experiments demonstrated that a minimum of eight animals was sufficient to determine statistical significance. Twelve mice therefore accounts for removal due to outliers, surgical complications, or inadequate fear acquisition. This experiment was repeated, and animals pooled across both instances to avoid the single cohort effect affecting statistical significance. Previous sequencing experiments have detected effect sizes of 1.2-1.5 fold with n = 6 samples per treatment. As we were unable to reach this in all sequencing experiments, this is discussed in this limitations section. For single molecule tracking, kymographs were generated with an n = 10 per group (one per dish) to minimise within-group variation. Each kymograph was constructed from approximately 12µm of dendrite, at a thickness of 1µm. Statistical analyses were generally one- and two-way ANOVAs accompanied by a post-hoc comparison between all groups and the relevant control group. For all short-read experiments, data was processed as follows:

1) Cutadapt (v3.7) was used to clip low-quality nucleotides and adapter sequences.

2) HISAT2 (v2.2.1) was used to align the reads against the mouse genome (mm10).

3) HTSeq-count (v2.0.5) was used to generate the count matrix for each sample.

4) edgeR (v4.4.1) was used for differential expression analysis between groups.

Results

Vaultrc5 is highly enriched at the synapse

A re-analysis of our previously published RNA-seq dataset (Wei et al, 2022) revealed a significant population of ncRNAs in the adult prefrontal cortex that are expressed in a subcellular compartment-specific manner (Figure 1A, B). Amongst the ncRNAs localised to the synapse, Gas5, Malat1, Rny1 and Rny3, and Vaultrc5 were the most abundant. We have previously demonstrated that synapse-enriched Gas5 and Malat1 are integral to fear learning (Liau et al., 2022; Madugalle et al., 2022). When Gas5 is knocked down at the synapse, Gas5-containing RNA granules are disassembled, which leads to increased intrinsic excitability and impaired fear extinction memory (Liau et al., 2022). Similarly, knockdown and targeted m6A demethylation of Malat1 at the synapse reduces its interaction with a group of novel m6A readers, which also impaired the formation of fear extinction (Madugalle et al., 2022). Rny1 and Rny3 have not been implicated in synaptic function, but have recently been shown to be glycosylated, and present on the outer cellular membrane.

Interestingly, Vaultrc5 expression was amongst the most dynamically expressed of all synapse enriched ncRNAs. In retention control mice it was eight times higher in the synapse than in the nucleus- a difference which was not present during fear extinction (Figure 1A, C). These data strongly suggest a role for Vaultrc5, and the accompanying ‘Vault’ ribonucleoprotein complex, in the regulation of synaptic plasticity and the formation of fear-related memory.

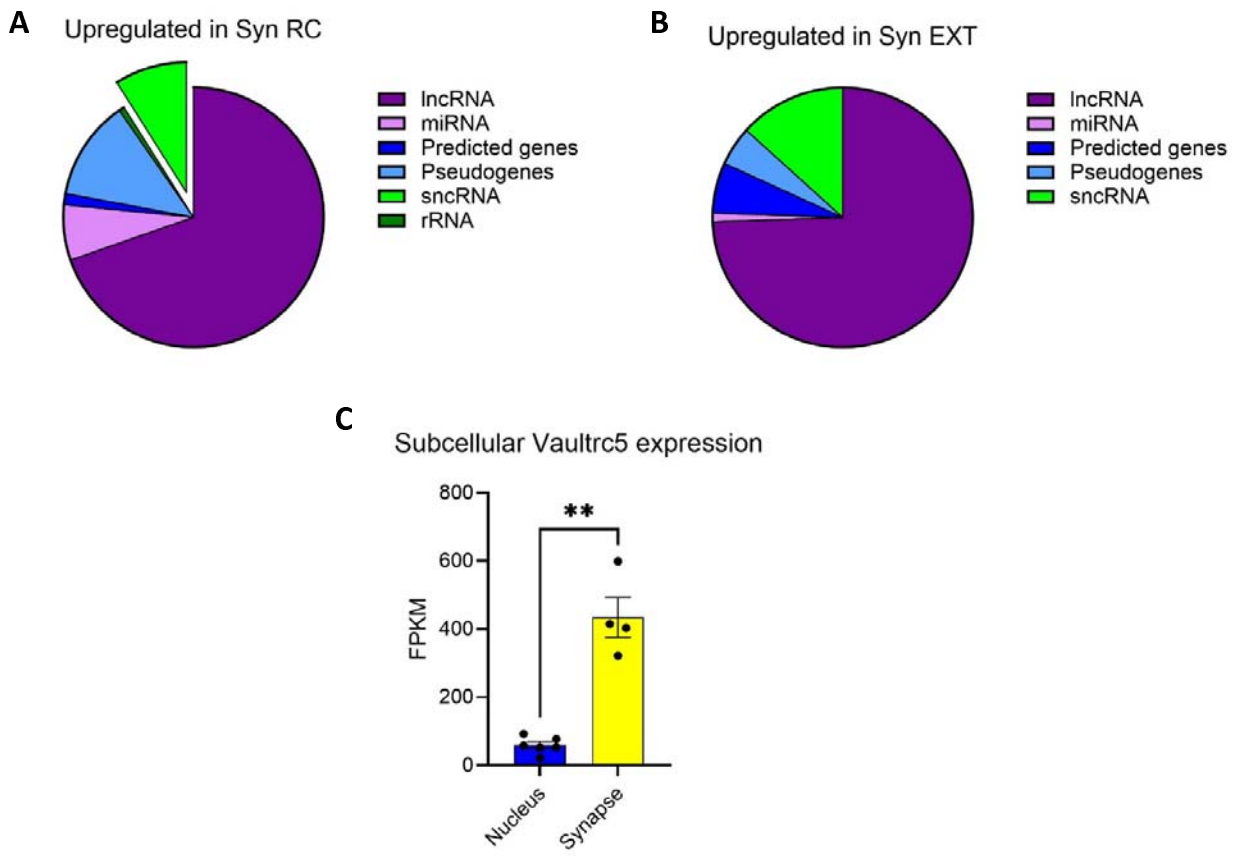

Figure 1 – Vaultrc5 is subcellularly localised in response to fear extinction learning. RNAseq data from fear-conditioned (EXT) or retention control (RC) mice, separated according to nuclear or synaptic (Syn) subcellular fraction. A-B) Classes of non-coding RNA found significantly upregulated at the synapse following (A) fear conditioning (retention control, RC) or (B) fear extinction learning (EXT). C) Read count (FPKM) of Vaultrc5 at the nucleus versus synapse. Unpaired two-tailed t-test with Welch's correction. Vaultrc5 is significantly upregulated in the synapse ($t = 6.321$, $df = 3.173$, $p = 0.0068$).

Vaults are most abundant in the presynaptic compartment, and their trafficking depends on Vaultrc5

Next, using STED microscopy to analyse the trafficking of Vaults in primary cortical neurons, *in vitro*, we measured the distribution of major vault protein MVP, and examined its colocalization with presynaptic and postsynaptic markers. Pre-synaptic terminals were identified using Bassoon (Fig 2A-D), and post synaptic terminals with Shank3 (E-H). For neurons stained with Bassoon (Fig 2A), images were taken using the axon terminal as a guide, while Shank3 (Fig 2E) used dendrites. We found that MVP was biased towards the

presynaptic terminal, which, given Vaultrc5's expression characteristics (Fig 1A, B), could indicate that Vaults spend transiting from the nucleus to the synapse.

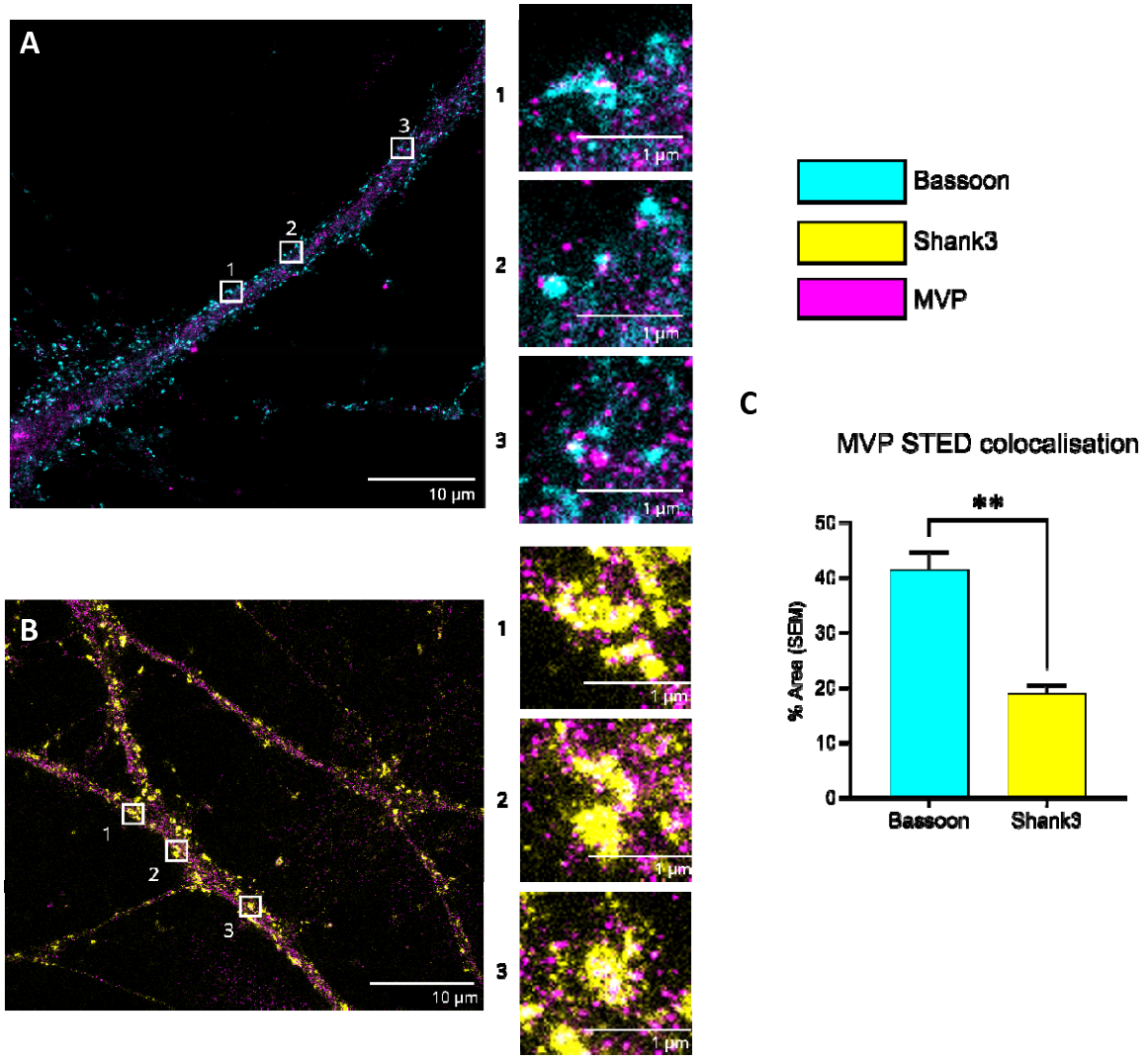

Figure 2 – MVP is presynaptically enriched. STED microscopy on DIV14 mouse primary cortical neurons. A) Representative presynaptic STED imagery using Bassoon (teal) and Major Vault Protein (MVP)(magenta). B) Representative postsynaptic STED imagery using Shank3 (teal) and MVP (magenta). C) Percent area of MVP colocalised with either Bassoon or Shank3. Unpaired two-tailed t-test with Welch's correction. Significantly more MVP was present at the presynapse, with a mean difference of 22.42 ± 4.66% ($t = 6.349$, $df = 4.068$, $p = 0.0029$).

We then used an MVP fused to GFP (MVP-GFP) fusion protein to tag vaults, and tracked them using kymography with a spinning-disc confocal microscope for 3 minutes at 2 frames per second (Fig 3A). Neurons were transfected with either the GFP tag, or the GFP tag plus a knockdown construct targeting Vaultrc5, and imaged under 20mM KCl-induced neuronal depolarisation conditions. After imaging, 12µm sections were processed using the

KymoClear 2.0 plugin for FIJI, splitting molecular movement into anterograde, retrograde, and pausing behaviour (Fig 3B).

Vaultrc5 knockdown led to a significant reduction in events per 10µm (Fig 3C). Knockdown did not impact run time per movement (Fig 3B), while pausing remained the most common, indicating that the effect on events per 10µm was not due to shorter movements. Velocity, and colocalization with pre and postsynaptic markers was not affected (Appendix). Considering Vaultrc5's high synaptic abundance, and these data, two possibilities arise; Vaultrc5 is only a passenger, and its functions in synaptic plasticity caused this disturbance in Vault movement or, Vaultrc5 knockdown has a "gear-shift" effect on Vaults, with knockdown leading to a switch to a more 'surveillance-focused' behaviour.

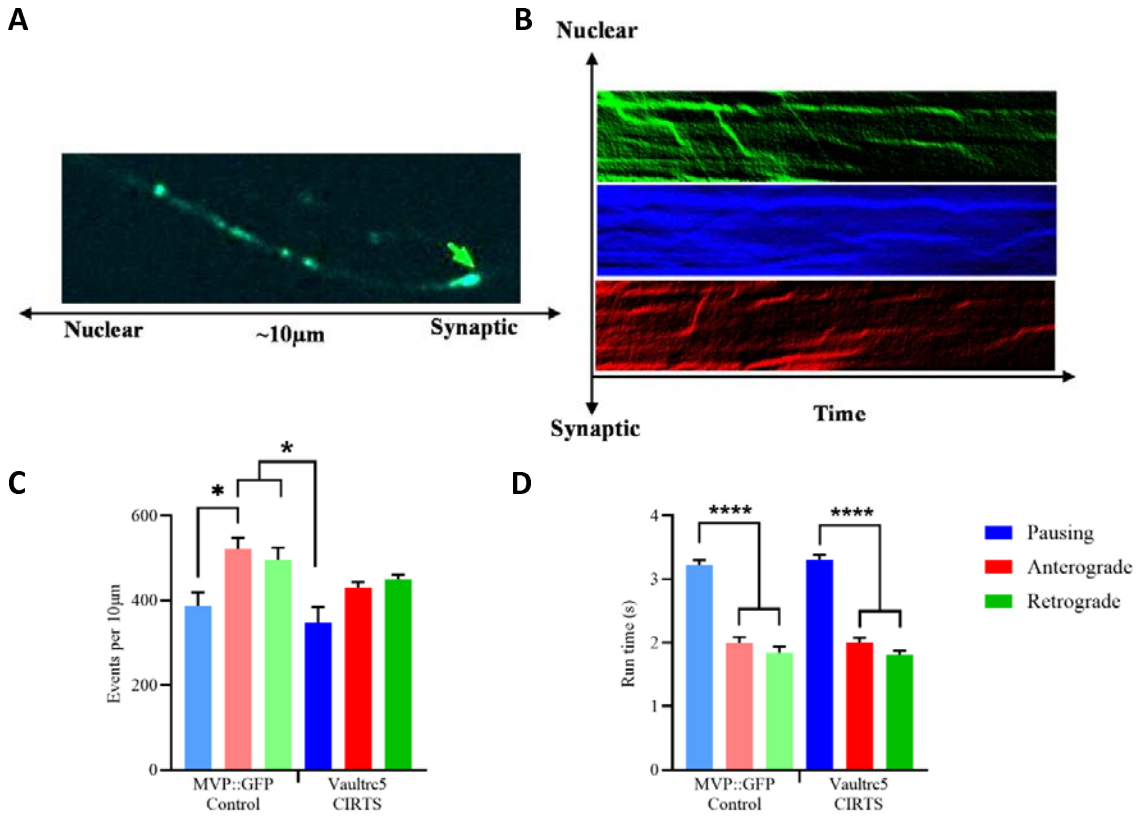

Figure 3 – Vault trafficking is attenuated by Vaultrc5 knockdown. Mouse primary cortical neuron (DIV7) kymographs of GFP-labelled vaults, with and without Vaultrc5 knockdown. Particles were tracked using a spinning-disk confocal for 3 minutes at 2 frames per second. One kymograph was generated per cell (n = 10). Videos were analysed using KymoClear 2.0 in ImageJ, then with one- and two-way ANOVA. A) Representative image taken from video used for kymograph in B. B) Representative kymograph of Vault trafficking. Anterograde (red), Pausing (blue), Retrograde (green). C) Events per 10µm per movement vector. Each event was one full path of a tracked molecule or molecular cluster. Pausing behaviour in the control group was significantly rarer than anterograde at 135.3 ± 57.79 events ($p = 0.011$). Pausing in the knockdown group was significantly less frequent than both control anterograde (164.6 ± 59.89, $p = 0.002$) and retrograde movement (138.5 ± 59.88, $p = 0.013$). D) Run time (s) per event. Both groups spent the most time pausing, at an average of 1.301 ($p < 0.0001$) for control, and 1.395 ($p < 0.0001$) for Vaultrc5 knockdown.

Vaults are trafficking granules

Having confirmed that Vaults are highly mobile in neuronal processes and that trafficking relies on Vaultrc5, we then examined the effect of Vaultrc5 on the Vault cargo in the nuclear and synaptic compartment. To address this, we immunoprecipitated Vaults from nuclear and synaptosome fractions derived from KCl-activated primary cortical neurons, and performed RNA sequencing on the Vault-enriched fractions.

Nuclear Vaults (Fig. 4A, C) contained primarily protein-coding transcripts, with small populations of lncRNAs, and unknown or uncharacterised transcripts. Most transcripts were involved in intercellular signalling and the immune response, including Meg3, a key lncRNA involved in learning, memory, and the immune response (Yi et al., 2019); Xist, required for X-chromosome dosage compensation(Sahakyan et al., 2018); and the major vault protein

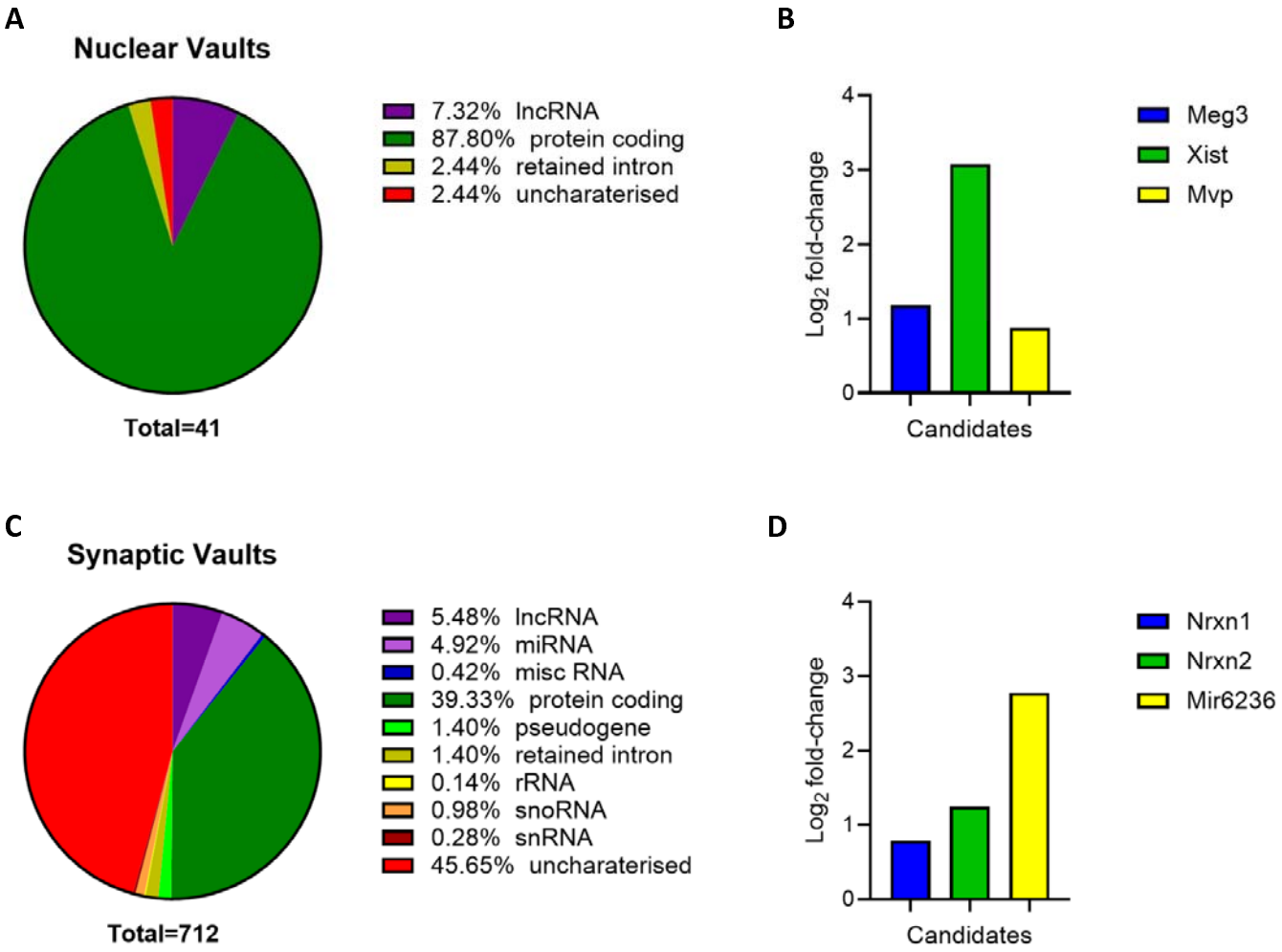

Figure 4 – Vault RNA cargo differs between the nucleus and synapse. Short-read sequencing reads of RNA derived from Vaults per subcellular compartment (n = 4 per compartment) under activated conditions. A, B) Transcripts found in Vaults derived from the nuclear compartment (n = 41), and example candidates: Meg3 ($q < 0.001$), Xist ($q < 0.001$), Mvp ($q = 0.014$). C,D) Transcripts found in Vaults derived from the synaptic compartment (n = 712), and selected candidates. Nrxn1 ($q < 0.001$), Nrxn2 ($q < 0.001$), miR-6236 ($q < 0.001$).

mRNA.

Synaptic Vaults (Fig. 4B, D) had a more than ten-fold increase in transcript diversity, with cargo split between uncharacterised and protein coding, with the majority being unknown. An array of smaller transcript populations was also present, primarily lncRNA and miRNA. Known transcripts included several involved in synaptic plasticity, such as Nrxn1 and 2, and miR6236. The neurexin family are well-known presynaptic cell adhesion proteins present throughout the nervous system (Lin et al., 2023), while miR6236 was recently shown to regulate neuronal repair and development (Chen et al., 2021). This is consistent with the idea that Vaults may play a role in synaptic modulation by trafficking transcripts required for the synapse to dynamically respond to environmental stimuli.

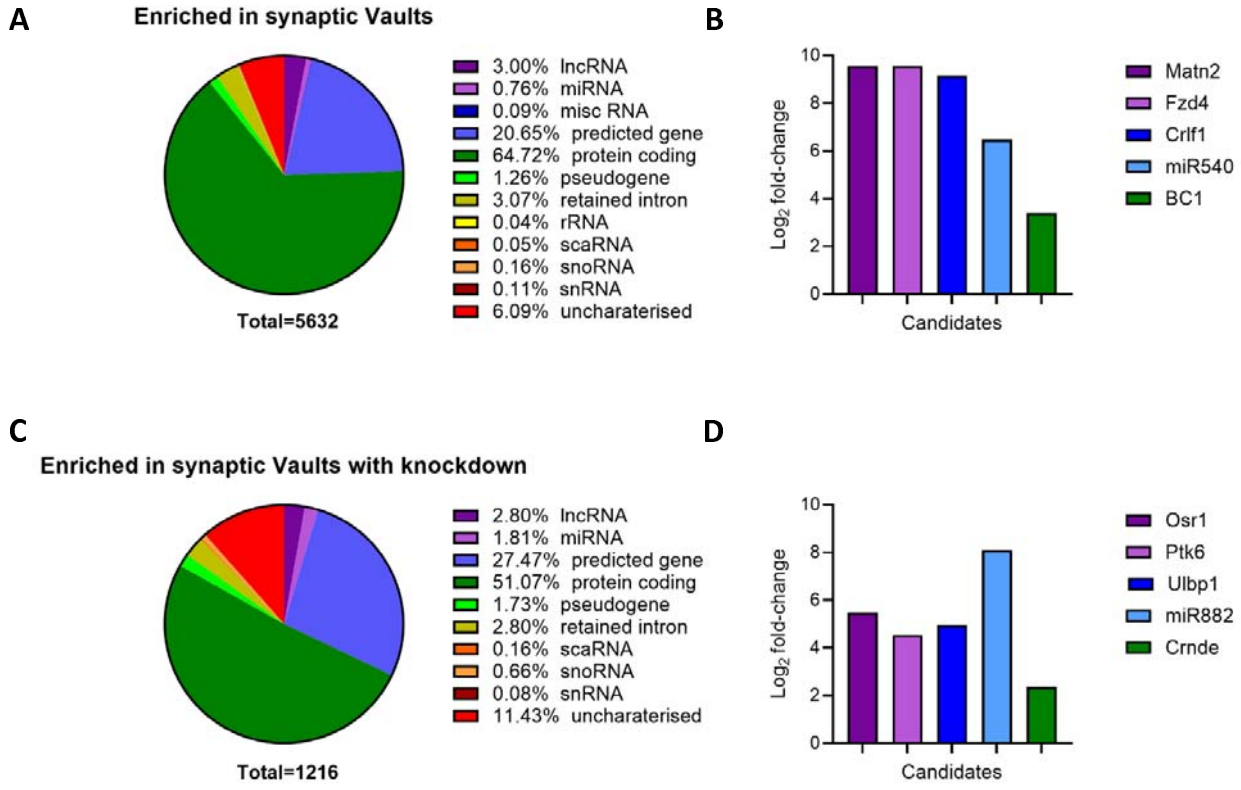

Figure 5 – Vaultrc5 acts as a "gear-shift" for Vault function. Short-read sequencing reads of RNA derived from Vaults per subcellular compartment (n = 4 per compartment) under activated conditions. Reads were analysed using pipeline described in methods, and background (IgG) subtracted from Vault immunoprecipitation. A,B) Transcripts enriched in synaptic Vaults (n = 5632 transcripts), with example transcripts: Matn2 ($q < 0.001$), Fzd4 ($q < 0.001$), Crlf1 ($q < 0.001$), miR-540 ($q < 0.001$), Bc1 ($q < 0.001$). C,D) Transcripts enriched in synaptic Vaults with knockdown (n = 1216 transcripts), with examples. Osr1 ($q = 0.005$), Ptk6 ($q < 0.001$), Ulbp1 ($q < 0.001$), miR-882 ($q < 0.001$), Crnde ($q = 0.048$).

Vaultrc5 regulates the content of synapse-enriched Vaults

Considering the increase in transcript diversity within Vaults enriched within the synaptic fraction, we examined the effect of Vaultrc5 knockdown on Vault cargo at the synapse. Vaultrc5 knockdown dramatically altered transcript diversity within the Vaults, with unknown, and immune signalling-related transcripts becoming more abundant. In addition, Vaaultrc5 knockdown produced many unaligned transcripts, the most abundant of which matched ribosomal, and mitochondrial RNA.

Most transcripts present in synaptic Vaults (Figure 5A, C) were mRNAs involved in cellular metabolism- primarily mitochondrial and ribosomal. Among these was the mRNA for Mtn2, neuroprotective in stroke (Sozmen et al., 2019); Fzd4, involved in dendrite morphogenesis (Bian et al., 2015); and Crlf1, a neurotrophic cytokine receptor ligand (Looyenga et al., 2013). Amongst the ncRNAs, we detected miR-540, which targets mRNA encoding voltage-dependent calcium channel, and is involved in stress-induced depression (Ma et al., 2016). Finally, we also identified BC1, a well-known lncRNA that regulates neuronal mRNA and results in impaired learning on the APA task (Chung et al., 2017).

With knockdown (Figure 5B, D), transcripts in synaptic Vaults shifted toward unknown and uncharacterised examples, with the most prevalent being immune signalling related. These included Osr1, a key transcription factor in nervous system development (Nugent et al., 2012); Ulbp1, a positive regulator of the adaptive immune response (Ruan et al., 2022); and Ptk6, a receptor tyrosine kinase involved in the innate immune response (Vlajic et al., 2024). For ncRNA there was miR-882, a promiscuous miRNA with many cell-cycle and cancer-related targets- one of which is Rev-erbα, a core component of the circadian clock (Griffin et al., 2019; Tian et al., 2021); and Crnde, which regulates the mTOR complex in cell growth and proliferation (Wang et al., 2015).

This variation in transcripts indicates that Vaultrc5 knockdown shifts the synaptic RNA pool towards processes involved in environmental signalling and the immune system, possibly by altering the compartment distribution of Vaults, or by affecting the transcripts being loaded within the Vaults. This would agree with precious work showing that MVP is upregulated in response to environmental signaling across infection, inflammation, and cancer (Mossink et al., 2003; Steiner et al., 2006)

Finally, the functional consequence of VaultRC5 knockdown at the synapse, *in vivo*, was explored. To do this, we used a lentiviral vector to deliver the Vaultrc5 knockdown construct to the infralimbic cortex of fear-conditioned mice, and examined its effect on fear extinction (Fig. 6A). Vaultrc5 knockdown led to significantly higher freezing scores during the first ten conditioned stimuli (CS) compared with controls (Fig. 6B). These data indicate a possible role for VaultRC5 in fear extinction learning. The higher freezing scores persisted during context B re-test, with no effect of VaultRC5 knockdown on extinction memory 24 hours after training (Fig. 6C). However, VaultRC5 knockdown led to a significant impairment in fear extinction memory when tested one week later (Fig. 6D). These data strongly suggest a regulatory role for Vaultrc5 in fear-related learning and memory. Whether this effect extends to other forms of learning or is active in other areas of the brain, remains to be determined.

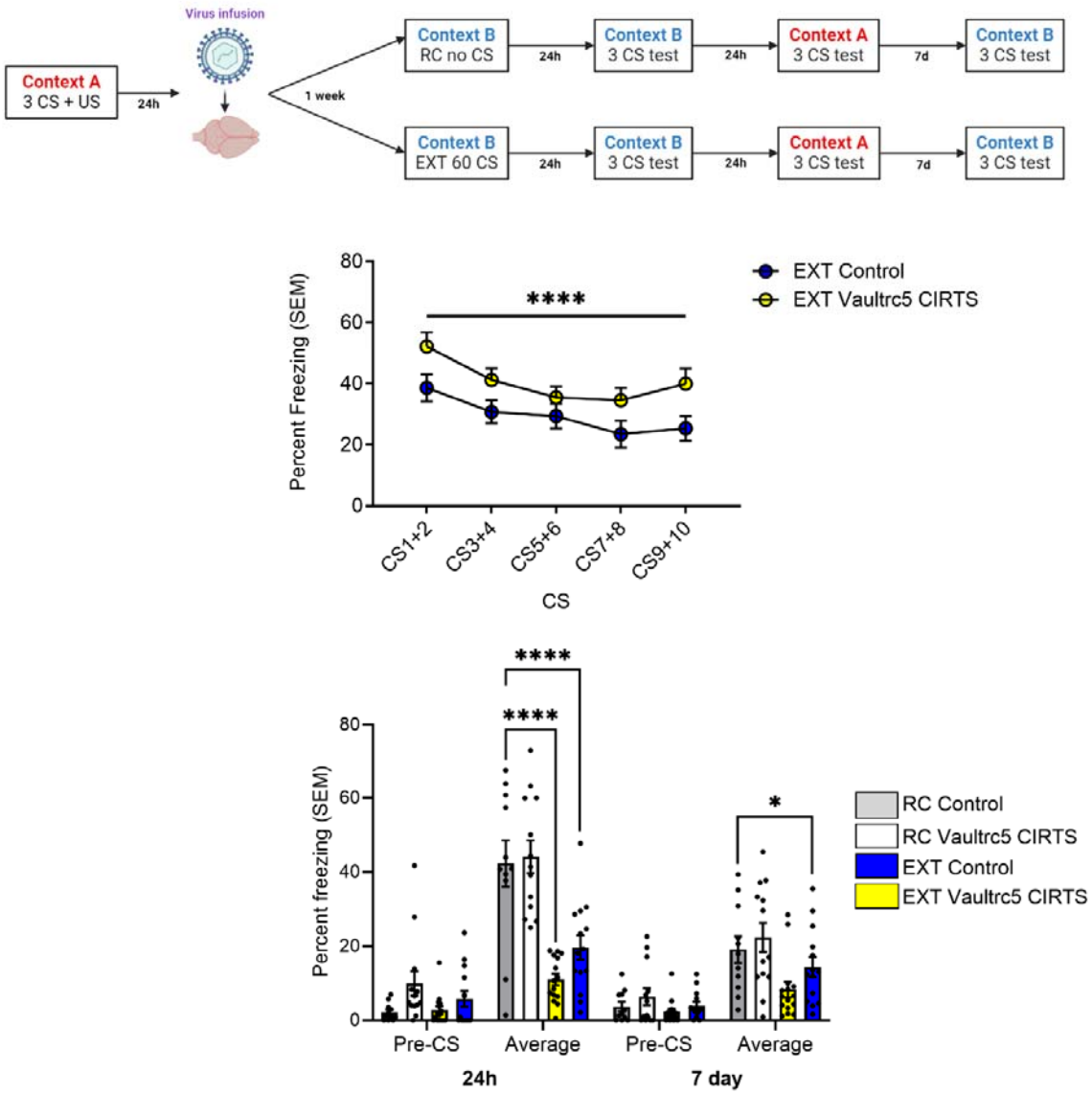

Figure 6 – Vaultrc5 knockdown impairs fear-related learning. A) Fear learning paradigm. CS = conditioned stimulus; US = unconditioned stimulus; RC = retention control, EXT = extinction. Mice were treated with either the control (GFP-targeting) or Vaultrc5-targeting CIRTS construct (n = 16-18 per group across 2 cohorts, 4 groups). Data are the percent time spent freezing in fear during testing ± the standard error in the mean, analysed by two-way ANOVA with Tukey's multiple comparisons test. B) Freezing score after either EXT or RC testing. Depleting Vaultrc5 significantly attenuated fear extinction within 10 CS repetitions, with a decrease in freezing score of 11.16 ± 4.984% ($F_{30,120}$ = 9.792, $p < 0.0001$). C) Mean freezing score in Context B after 3 CS, one day and one week post fear extinction. At 24h later, both EXT groups had significantly lower freezing than the respective RC group. RC Control vs EXT Control decreased freezing by 31.19 ± 5.99%. RC Vaultrc5 vs EXT Vaultrc5 decreased freezing by 24.45 ± 5.82%. At 7 days later, RC GFP vs EXT GFP had significantly decreased freezing, at 10.77 ± 4.61%.

A

Discussion

Since their discovery in 1986, Vaults have been considered to be large, empty, nanoparticles that could be useful as drug delivery vehicles (Casanas et al., 2012; Kedersha & Rome, 1986). In this study, we have demonstrated that Vaults are far more complex than previously assumed. We have found that 1) Vaults are trafficking granules that shuttle RNA between the soma and synapse, a process that requires the noncoding RNA Vaultrc5; 2) Knocking down Vaultrc5 causes the Vault's cargo to switch to a population of more metabolic, and immune signal-responsive transcripts; and 3) Vaultrc5 knockdown impairs fear-related learning and long-term memory. Taken together, these data indicate that neuronal Vaults and Vaultrc5 respond dynamically to environmental cues, and are integral to the regulation of RNA metabolism underlying learning and memory.

The finding that Vaults are trafficking granules is the first evidence of Vault function in any context. Early studies on Vaults had not examined their RNA cargo due to technological limitations, so they were assumed empty. Further, previous studies had linked MVP and Vaultrc5 to the immune system and synaptic plasticity, but were unable to link these characteristics to Vault function. Here, we show that Vaults are present in both the pre- and post-synaptic compartment, albeit with a bias toward presynaptic trafficking, and that the Vault's transcript cargo changes in response to its environmental context, including the subcellular compartment.

Synaptic compared to nuclear Vaults had a far more diverse transcriptome, with the majority being uncharacterised, then protein-coding. Nuclear Vaults primarily contained mRNA, and several kinds of ncRNA. These included the MVP mRNA, Meg3, and Xist, all of which are extensively implicated in intercellular signalling and the immune system. Some of the most common transcripts in synaptic Vaults were miR-6236, and Neurexins 1 and 2. MiR-6236 was recently shown to regulate neuronal repair and development, while the neurexin family are presynaptic adhesion proteins well-characterised as key to synaptic function. The shift in content and function, and the presence of these specific transcripts, confirm that Vaults function as trafficking granules in synaptic modulation.

Our data indicating that Vaultrc5 is required for both Vault movement and content ties into previous studies indicating that Vaultrc5 has at least two synaptic functions: 1) It is associated with the SQSTM1 complex in autophagy, and 2) both Vaultrc5 and MVP are critical to in MAPK/ERK activation at the neurite in synaptogenesis. Here we show that Vaultrc5 knockdown in synaptic Vaults leads to a marked accumulation of unaligned reads, unknown transcripts and RNA involved in metabolic, and immune-related signalling, including Ulbp1, Ptk6, and miR-882. Ulbp1 and Ptk6 are regulators of the adaptive, and innate immune response, respectively. miR-882 is a promiscuous miRNA with many cell cycle-related targets- one of which was Rev-erbα, key to the circadian clock and a regulator of inflammation. The shift in synaptic Vault cargo towards immune signalling-related RNAs suggests that Vaultrc5 acts as a "gear shift", with its downregulation causing Vaults to become more receptive to environmental signals. This would fit with the altered movement and extended pausing behaviour of Vaults caused by Vaultrc5 knockdown. Thus, Vaults appear to monitor, and respond to environmental changes by substituting the cargo they deliver to the synapse. This surveillance function of the Vault could be mediated by Vaultrc5 itself, or other miRNAs. miRNA are well-characterised as immune rheostats- fine-tuners of the cellular environment, where small changes in their expression, or binding partner accessibility, has large and varied downstream, and recursive upstream effects. One prominent example is miR-181, which is also within synaptic Vaults, and controls early

natural killer T cell development (Henao-Mejia et al., 2013). Interestingly, Vaultrc5 undergoes NSUN2 methylation-dependent, DICER-mediated processing into several miRNA-like small Vault RNAs (svtRNAs). These svtRNAs have been shown to act like miRNA in immune function and disease- for example, svtRNA2-1 is upregulated early in Parkinson's disease, perturbing cellular metabolism (Minones-Moyano et al., 2013). The signal for their production has not been elucidated but, given our data on synaptic Vaults following Vaultrc5 knockdown, their presence could be due to Vaultrc5 fine-tuning the Vault to respond to environmental signalling.

The interaction between the Vault and Vaultrc5 likely underlies the behavioural phenotype. Vaultrc5 knockdown prior to fear extinction affected the rate at which mice were able to dissociate the conditioned and unconditioned stimulus, both in-session and in the context re-tests. Given the observation that Vaultrc5 enables the Vault to respond to environmental signalling, knockdown may have reduced the intrinsic excitability of neurons prior to fear extinction. A less plastic state would indicate that the Vaults' response of switching to metabolic and immune-related transcripts may lead the neurons away from an activatable state, focusing their activity instead on processes involved environmental sensing.

A reduction in intrinsic excitability could arise from the fact that both Vaultrc5, and MVP interact with the MAPK/ERK pathway at the synapse. First, the EF-hand motif present on MVP is generally known to interact with both pH, and intracellular Ca^{2+}, with pH being implicated in Vault opening (Lin et al., 2021; Querol-Audi et al., 2009). Vaultrc5 activating the MAPK pathway could increase MVP's phosphorylation levels, providing another trigger for Vault opening other than synaptic transmission. Fewer open Vaults combined with less MAPK/ERK activation, leading to decreased synaptic plasticity (Bluthgen et al., 2017), could result in an overbalance of Vaults carrying immune signalling-related transcripts.

In summary, we have discovered that Vaults are trafficking granules involved in moving RNA cargo between the neuron soma and synapse, which depend on the activity of Vaultrc5. Vaultrc5 may thus act as a gear-shift to fine-tune the Vault's response to environmental signalling, with consequential effects on experience-dependent plasticity, learning, and memory.

Acknowledgements. We gratefully acknowledge grant support from the Brain and Behavioral Research Foundation (NARSAD Independent Investigator Award, T.W.B.) and NHMRC Ideas Grant (GNT2003414) to T.W.B. L.J.L. S.U.M. and E.L.Z. were supported by a Westpac Future Scholarship and the University of Queensland. M.M. was supported by the Australian Research Training Stipend. We thank the Queensland Brain Institute Advanced Microscopy Facility for its support and Ms. Rowan Tweedale for manuscript editing.

The authors declare that they have no conflict of interest.

Antar, L. N., Dictenberg, J. B., Plociniak, M., Afroz, R., & Bassell, G. J. (2005). Localization of FMRP-associated mRNA granules and requirement of microtubules for activity-dependent trafficking in hippocampal neurons. *Genes Brain Behav*, *4*(6), 350-359. https://doi.org/10.1111/j.1601-183X.2005.00128.x

Autour, A., S, C. Y. J., A, D. C., Abdolahzadeh, A., Galli, A., Panchapakesan, S. S. S., Rueda, D., Ryckelynck, M., & Unrau, P. J. (2018). Fluorogenic RNA Mango aptamers for imaging small non-coding RNAs in mammalian cells. *Nat Commun*, *9*(1), 656. https://doi.org/10.1038/s41467-018-02993-8

Bian, W. J., Miao, W. Y., He, S. J., Wan, Z. F., Luo, Z. G., & Yu, X. (2015). A novel Wnt5a-Frizzled4 signaling pathway mediates activity-independent dendrite morphogenesis via the distal PDZ motif of Frizzled 4. *Dev Neurobiol*, *75*(8), 805-822. https://doi.org/10.1002/dneu.22250

Bluthgen, N., van Bentum, M., Merz, B., Kuhl, D., & Hermey, G. (2017). Profiling the MAPK/ERK dependent and independent activity regulated transcriptional programs in the murine hippocampus in vivo. *Sci Rep*, *7*, 45101. https://doi.org/10.1038/srep45101

Casanas, A., Guerra, P., Fita, I., & Verdaguer, N. (2012). Vault particles: a new generation of delivery nanodevices. *Curr Opin Biotechnol*, *23*(6), 972-977. https://doi.org/10.1016/j.copbio.2012.05.004

Chen, C., Hardy, M., Zhang, J., LaHoste, G. J., & Bazan, N. G. (2006). Altered NMDA receptor trafficking contributes to sleep deprivation-induced hippocampal synaptic and cognitive impairments. *Biochem Biophys Res Commun*, *340*(2), 435-440. https://doi.org/10.1016/j.bbrc.2005.12.021

Chen, Y.-J., Huang, Y.-A., Ho, C. T., Yang, J.-M., Chao, J.-I., Li, M.-C., & Hwang, E. (2021). A Nanodiamond-Based Surface Topography Downregulates the MicroRNA miR6236 to Enhance Neuronal Development and Regeneration. *ACS Applied Bio Materials*, *4*(1), 890-902. https://doi.org/10.1021/acsabm.0c01389

Chung, A., Dahan, N., Alarcon, J. M., & Fenton, A. A. (2017). Effects of regulatory BC1 RNA deletion on synaptic plasticity, learning, and memory. *Learn Mem*, *24*(12), 646-649. https://doi.org/10.1101/lm.045617.117

Doyle, M., & Kiebler, M. A. (2011). Mechanisms of dendritic mRNA transport and its role in synaptic tagging. *EMBO J*, *30*(17), 3540-3552. https://doi.org/10.1038/emboj.2011.278

Dunkley, P. R., Jarvie, P. E., & Robinson, P. J. (2008). A rapid Percoll gradient procedure for preparation of synaptosomes. *Nat Protoc*, *3*(11), 1718-1728. https://doi.org/10.1038/nprot.2008.171

Griffin, P., Dimitry, J. M., Sheehan, P. W., Lananna, B. V., Guo, C., Robinette, M. L., Hayes, M. E., Cedeno, M. R., Nadarajah, C. J., Ezerskiy, L. A., Colonna, M., Zhang, J., Bauer, A. Q., Burris, T. P., & Musiek, E. S. (2019). Circadian clock protein Rev-erbalpha regulates neuroinflammation. *Proc Natl Acad Sci U S A*, *116*(11), 5102-5107. https://doi.org/10.1073/pnas.1812405116

Henao-Mejia, J., Williams, A., Goff, L. A., Staron, M., Licona-Limon, P., Kaech, S. M., Nakayama, M., Rinn, J. L., & Flavell, R. A. (2013). The microRNA miR-181 is a critical cellular metabolic rheostat essential for NKT cell ontogenesis and lymphocyte development and homeostasis. *Immunity*, *38*(5), 984-997. https://doi.org/10.1016/j.immuni.2013.02.021

Hirokawa, N. (2006). mRNA transport in dendrites: RNA granules, motors, and tracks. *J Neurosci*, *26*(27), 7139-7142. https://doi.org/10.1523/JNEUROSCI.1821-06.2006

Kang, H., & Schuman, E. M. (1996). A requirement for local protein synthesis in neurotrophin-induced hippocampal synaptic plasticity. *Science*, *273*(5280), 1402-1406. https://doi.org/10.1126/science.273.5280.1402

Kedersha, N. L., & Rome, L. H. (1986). Isolation and characterization of a novel ribonucleoprotein particle: large structures contain a single species of small RNA. *J Cell Biol*, *103*(3), 699-709. https://doi.org/10.1083/jcb.103.3.699

Kiebler, M. A., & DesGroseillers, L. (2000). Molecular insights into mRNA transport and local translation in the mammalian nervous system. *Neuron*, *25*(1), 19-28. https://doi.org/10.1016/s0896-6273(00)80868-5

Knowles, R. B., Sabry, J. H., Martone, M. E., Deerinck, T. J., Ellisman, M. H., Bassell, G. J., & Kosik, K. S. (1996). Translocation of RNA granules in living neurons. *J Neurosci*, *16*(24), 7812-7820. https://www.ncbi.nlm.nih.gov/pubmed/8987809

Koenig, E., Martin, R., Titmus, M., & Sotelo-Silveira, J. R. (2000). Cryptic peripheral ribosomal domains distributed intermittently along mammalian myelinated axons. *J Neurosci*, *20*(22), 8390-8400. https://www.ncbi.nlm.nih.gov/pubmed/11069946

Liau, W.-S., Zhao, Q., Bademosi, A., Gormal, R., Gong, H., Marshall, P. R., Periyakaruppiah, A., Madugalle, S. U., Zajackowski, E. L., Leighton, L. J., Ren, H., Musgrove, M., Davies, J., Rauch, S., He, C., Dickinson, B. C., Li, X., Wei, W., Meunier, F. A.,…Bredy, T. W. (2022). Fear extinction is regulated by long noncoding RNA activity at the synapse. *bioRxiv*, 2022.2003.2030.486308. https://doi.org/10.1101/2022.03.30.486308

Lin, P. Y., Chen, L. Y., Jiang, M., Trotter, J. H., Seigneur, E., & Sudhof, T. C. (2023). Neurexin-2: An inhibitory neurexin that restricts excitatory synapse formation in the hippocampus. *Sci Adv*, *9*(1), eadd8856. https://doi.org/10.1126/sciadv.add8856

Lin, Q. T., Lee, R., Feng, A. L., Kim, M. S., & Stathopulos, P. B. (2021). The leucine zipper EF-hand containing transmembrane protein-1 EF-hand is a tripartite calcium, temperature, and pH sensor. *Protein Sci*, *30*(4), 855-872. https://doi.org/10.1002/pro.4042

Looyenga, B. D., Resau, J., & MacKeigan, J. P. (2013). Cytokine receptor-like factor 1 (CRLF1) protects against 6-hydroxydopamine toxicity independent of the gp130/JAK signaling pathway. *PLoS One*, *8*(6), e66548. https://doi.org/10.1371/journal.pone.0066548

Ma, K., Guo, L., Xu, A., Cui, S., & Wang, J. H. (2016). Molecular Mechanism for Stress-Induced Depression Assessed by Sequencing miRNA and mRNA in Medial Prefrontal Cortex. *PLoS One*, *11*(7), e0159093. https://doi.org/10.1371/journal.pone.0159093

Madugalle, S. U., Liau, W.-S., Zhao, Q., Li, X., Gong, H., Marshall, P. R., Periyakaruppiah, A., Zajackowski, E. L., Leighton, L. J., Ren, H., Musgrove, M., Davies, J., Rauch, S., He, C., Dickinson, B. C., Fletcher, L., Fulopova, B., Williams, S. R., Spitale, R. C., & Bredy, T. W. (2022). Discovery of synapse-specific RNA N6-methyladenosine readers associated with the consolidation of fear extinction memory. *bioRxiv*, 2022.2006.2007.495230. https://doi.org/10.1101/2022.06.07.495230

Marshall, P. R., Davies, J., Zhao, Q., Liau, W. S., Lee, Y., Basic, D., Periyakaruppiah, A., Zajaczkowski, E. L., Leighton, L. J., Madugalle, S. U., Musgrove, M., Kielar, M., Brueckner, A. M., Gong, H., Ren, H., Walsh, A., Kaczmarczyk, L., Jackson, W. S., Chen, A.,…Bredy, T. W. (2024). DNA G-Quadruplex Is a Transcriptional Control Device That Regulates Memory. *J Neurosci*, *44*(15). https://doi.org/10.1523/JNEUROSCI.0093-23.2024

Mathur, C., Johnson, K. R., Tong, B. A., Miranda, P., Srikumar, D., Basilio, D., Latorre, R., Bezanilla, F., & Holmgren, M. (2018). Demonstration of ion channel synthesis by isolated squid giant axon provides functional evidence for localized axonal membrane protein translation. *Sci Rep*, *8*(1), 2207. https://doi.org/10.1038/s41598-018-20684-8

Minones-Moyano, E., Friedlander, M. R., Pallares, J., Kagerbauer, B., Porta, S., Escaramis, G., Ferrer, I., Estivill, X., & Marti, E. (2013). Upregulation of a small vault RNA (svtRNA2-1a) is an early event in Parkinson disease and induces neuronal dysfunction. *RNA Biol*, *10*(7), 1093-1106. https://doi.org/10.4161/rna.24813

Mossink, M. H., van Zon, A., Scheper, R. J., Sonneveld, P., & Wiemer, E. A. (2003). Vaults: a ribonucleoprotein particle involved in drug resistance? *Oncogene*, *22*(47), 7458-7467. https://doi.org/10.1038/sj.onc.1206947

Nugent, B. M., Valenzuela, C. V., Simons, T. J., & McCarthy, M. M. (2012). Kinases SPAK and OSR1 are upregulated by estradiol and activate NKCC1 in the developing hypothalamus. *J Neurosci*, *32*(2), 593-598. https://doi.org/10.1523/JNEUROSCI.5415-11.2012

Paspalas, C. D., Perley, C. C., Venkitaramani, D. V., Goebel-Goody, S. M., Zhang, Y., Kurup, P., Mattis, J. H., & Lombroso, P. J. (2009). Major vault protein is expressed along the nucleus-neurite axis and associates with mRNAs in cortical neurons. *Cereb Cortex*, *19*(7), 1666-1677. https://doi.org/10.1093/cercor/bhn203

Poderycki, M. J., Kickhoefer, V. A., Kaddis, C. S., Raval-Fernandes, S., Johansson, E., Zink, J. I., Loo, J. A., & Rome, L. H. (2006). The vault exterior shell is a dynamic structure that allows incorporation of vault-associated proteins into its interior. *Biochemistry*, *45*(39), 12184-12193. https://doi.org/10.1021/bi0610552

Querol-Audi, J., Casanas, A., Uson, I., Luque, D., Caston, J. R., Fita, I., & Verdaguer, N. (2009). The mechanism of vault opening from the high resolution structure of the N-terminal repeats of MVP. *EMBO J*, *28*(21), 3450-3457. https://doi.org/10.1038/emboj.2009.274

Rangaraju, V., Tom Dieck, S., & Schuman, E. M. (2017). Local translation in neuronal compartments: how local is local? *EMBO Rep*, *18*(5), 693-711. https://doi.org/10.15252/embr.201744045

Ruan, G. T., Xie, H. L., Zhu, L. C., Ge, Y. Z., Yan, L., Liao, C., Gong, Y. Z., & Shi, H. P. (2022). Immune ULBP1 is Elevated in Colon Adenocarcinoma and Predicts Prognosis. *Front Genet*, *13*, 762514. https://doi.org/10.3389/fgene.2022.762514

Sahakyan, A., Yang, Y., & Plath, K. (2018). The Role of Xist in X-Chromosome Dosage Compensation. *Trends Cell Biol*, *28*(12), 999-1013. https://doi.org/10.1016/j.tcb.2018.05.005

Sossin, W. S., & DesGroseillers, L. (2006). Intracellular trafficking of RNA in neurons. *Traffic*, *7*(12), 1581-1589. https://doi.org/10.1111/j.1600-0854.2006.00500.x

Sozmen, E. G., DiTullio, D. J., Rosenzweig, S., Hinman, J. D., Bridges, S. P., Marin, M. A., Kawaguchi, R., Coppola, G., & Carmichael, S. T. (2019). White Matter Stroke Induces a Unique Oligo-Astrocyte Niche That Inhibits Recovery. *J Neurosci*, *39*(47), 9343-9359. https://doi.org/10.1523/JNEUROSCI.0103-19.2019

Steiner, E., Holzmann, K., Elbling, L., Micksche, M., & Berger, W. (2006). Cellular functions of vaults and their involvement in multidrug resistance. *Curr Drug Targets*, *7*(8), 923-934. https://doi.org/10.2174/138945006778019345

Steward, O., & Levy, W. B. (1982). Preferential localization of polyribosomes under the base of dendritic spines in granule cells of the dentate gyrus. *J Neurosci*, *2*(3), 284-291. https://www.ncbi.nlm.nih.gov/pubmed/7062109

Tian, Y., Gong, Z., Zhao, R., & Zhu, Y. (2021). Melatonin inhibits RANKL-induced osteoclastogenesis through the miR-882/Rev-erbalpha axis in Raw264.7 cells. *Int J Mol Med*, *47*(2), 633-642. https://doi.org/10.3892/ijmm.2020.4820

van Zon, A., Mossink, M. H., Schoester, M., Scheffer, G. L., Scheper, R. J., Sonneveld, P., & Wiemer, E. A. (2002). Structural domains of vault proteins: a role for the coiled coil domain in vault assembly. *Biochem Biophys Res Commun*, *291*(3), 535-541. https://doi.org/10.1006/bbrc.2002.6472

Vlajic, K., Bie, W., Gilic, M. B., & Tyner, A. L. (2024). Impaired activation of succinate-induced type 2 immunity and secretory cell production in the small intestines of Ptk6-/- male mice. *Cell Death Dis*, *15*(10), 777. https://doi.org/10.1038/s41419-024-07149-9

Wakatsuki, S., Takahashi, Y., Shibata, M., Adachi, N., Numakawa, T., Kunugi, H., & Araki, T. (2021). Small noncoding vault RNA modulates synapse formation by amplifying MAPK signaling. *J Cell Biol*, *220*(2). https://doi.org/10.1083/jcb.201911078

Wang, Y., Wang, Y., Li, J., Zhang, Y., Yin, H., & Han, B. (2015). CRNDE, a long-noncoding RNA, promotes glioma cell growth and invasion through mTOR signaling. *Cancer Lett*, *367*(2), 122-128. https://doi.org/10.1016/j.canlet.2015.03.027

Yi, J., Chen, B., Yao, X., Lei, Y., Ou, F., & Huang, F. (2019). Upregulation of the lncRNA MEG3 improves cognitive impairment, alleviates neuronal damage, and inhibits activation of astrocytes in hippocampus tissues in Alzheimer's disease through inactivating the PI3K/Akt signaling pathway. *J Cell Biochem*, *120*(10), 18053-18065. https://doi.org/10.1002/jcb.29108